DALTON
FULL PAPER

Chloro(*N*-*p*-nitrobenzoylimido-*meso*-tetraphenylporphyrinato)iron(III): a high-spin complex †

Ching-Huei Chen,[a] Yu-Yi Lee,[a] Bing-Chuang Liau,[a] Shanmugham Elango,[a] Jyh-Horung Chen,*[a] Hsi-Ying Hsieh,[b] Feng-Ling Liao,[c] Sue-Lein Wang[c] and Lian-Pin Hwang[d]

[a] *Department of Chemistry, National Chung-Hsing University, Taichung 40227, Taiwan*
[b] *Chung Hwa College of Medical Technology, Tainan 717, Taiwan*
[c] *Department of Chemistry, National Tsing-Hua University, Hsin-Chu 30043, Taiwan*
[d] *Department of Chemistry, National Taiwan University and Institute of Atomic and Molecular Sciences, Academia Sinica, Taipei 10764, Taiwan*

Received 20th March 2002, Accepted 29th May 2002
First published as an Advance Article on the web 4th July 2002

The crystal structures of diamagnetic (methanol)(*N*-*p*-nitrobenzoylimido-*meso*-tetraphenylporphyrinato)zinc(II) methanol solvate Zn(N-*p*-$NCOC_6H_4NO_2$-tpp)(MeOH)·MeOH [or **4**(MeOH)·MeOH] and paramagnetic chloro-(*N*-*p*-nitrobenzoylimido-*meso*-tetraphenylporphyrinato)iron(III) Fe(N-*p*-$NCOC_6H_4NO_2$-tpp)Cl (**5**), were determined. Both are pentacoordinate complexes where the *p*-nitrobenzoylimido (NNB) moiety is inserted into a zinc–pyrrole (or iron–pyrrole) bond. The coordination geometry of the zinc (or iron) center is best described as a distorted trigonal bipyramid with the N(2), N(5), and O(4) [or N(2), N(5), and Cl(1)] atoms lying in the equatorial plane. The plane of the three pyrrole nitrogen atoms [*i.e.*, N(1), N(2) and N(3)] strongly bonded to Zn^{2+} in **4**(MeOH)·MeOH (or Fe^{3+} in **5**) is adopted as a reference plane, 3N. The porphyrin ring is severely distorted and the pyrrole ring N(4) is bonded to the NNB ligand making a dihedral angle of 30.0° (or 27.8°) with the 3N plane for **4**(MeOH)·MeOH (or **5**). Solid state magnetic susceptibility and the effective magnetic moment data were measured for **5** from 300 to 5 K. In the higher temperature range ($T > 50$ K), the effective magnetic moment is constant and is equal to 5.87 μ_B. This μ_{eff} value confirms that there is a high-spin ferric ($S = 5/2$) state for the iron atom in **5**. The *g* values of 9.5 ± 0.4, 4.2 and 1.1 measured from X-band EPR spectra were also consistent with a high-spin ferric iron in **5**. The magnitude of zero field splitting, *D*, and the rhombicity parameter, λ (= *E*/*D*), in **5** were determined approximately as 0.79 cm^{-1} and 0.29, respectively, by EPR spectroscopy and paramagnetic susceptibility measurements.

Introduction

Metalloporphyrins with a bridged structure between the central metal and one of the four pyrrole nitrogens are of great interest since an iron(III) porphyrin with an oxygen atom inserted into an Fe–N bond is postulated as one of the possible structures for the highly oxidized forms of some hemoproteins.[1] Many bridged metalloporphyrins with metal–NTs–N linkages (metal = Zn,[2] Ni,[3] Fe,[4] Hg,[5] Ga,[6] Tl;[6] Ts = tosyl) have so far been reported. Callot *et al.*[3] reported the synthesis and spectroscopic characterization of the metallation of *N*-*p*-nitrobenzoylamido-*meso*-tetraphenylporphyrin [N-*p*-$HNCOC_6H_4NO_2$-Htpp] (tpp = the dianion of *meso*-tetraphenylporphyrin) leading to mononuclear complexes of (*N*-*p*-nitrobenzoylimido-*meso*-tetraphenylporphyrinato)nickel(II) Ni(N-*p*-$NCOC_6H_4NO_2$-tpp) (**1**) and (*N*-*p*-nitrobenzoylimido-*meso*-tetraphenylporphyrinato)-copper(II) Cu(N-*p*-$NCOC_6H_4NO_2$-tpp) (**2**). We have recently reported the X-ray structures of two diamagnetic, mononuclear, and bridged metal complexes *i.e.*, the four-coordinate compound of **1** and the six-coordinate complex of *cis*-acetato(*N*-*p*-nitrobenzoylimido-*meso*-tetraphenylporphyrinato)-thallium(III) Tl(N-*p*-$NCOC_6H_4NO_2$-tpp)(OAc) (**3**).[7]

In this paper, we present the results obtained upon replacing Ni(II) with Zn(II) and Fe(III) in **1** forming new compounds **4**(MeOH)·MeOH and **5**, respectively. This replacement increases the coordination number (CN) from 4 of **1** to 5 forming diamagnetic (methanol)(*N*-*p*-nitrobenzoylimido-*meso*-tetraphenylporphyrinato)zinc(II) methanol solvate Zn(N-*p*-$NCOC_6H_4NO_2$-tpp) [or **4**(MeOH)·MeOH] and paramagnetic chloro-*N*-*p*-nitrobenzoylimido-*meso*-tetraphenylporphyrinato-iron(III) Fe(N-*p*-$NCOC_6H_4NO_2$-tpp)Cl (**5**). Compound **5**, like a wide variety of neutral five-coordinate ferric porphyrin complexes, Fe(por)X (X^- = an anionic ligand), can have a low- (S = 1/2), intermediate- (S = 3/2) or high-spin (S = 5/2), or quantum mechanically spin-admixed (S = 3/2, 5/2) ground state, depending on the ligand field strength of the anion.[8] Although the data for Fe(N–NTs–tpp)Cl was published 14 years ago by Mansuy and co-workers,[4] there was some ambiguity in the intepretation and assignment of their EPR data. Futhermore, the replacement of tosylimido (NTs) substituents in Fe(N-NTs-tpp)Cl by *N*-*p*-nitrobenzoylimido (NNB) ligand in compound **5** provides a route to observe the zero-field splitting parameter, *D*, and the rhombicity parameter, λ (= *E*/*D*), for **5** by X-band EPR spectroscopy and paramagnetic susceptibility mesurements. We report herein the X-ray structures of **4**(MeOH)·MeOH and **5** and the analysis of the electronic and magnetic properties of **5** from magnetic susceptibility mearsurements and EPR and ^1H NMR spectroscopic studies. Complex **5** is the first example of an iron(III) porphyrin with high-spin (S = 5/2) which has the Fe^{III}–N–(*p*-$COC_6H_4NO_2$)–N (or Fe–NNB–N) linkage.

Experimental

Preparation of Zn(N-*p*-$NCOC_6H_4NO_2$-tpp) (4)

Compound **4** was prepared in the same way as described for Ni(N-*p*-$NCOC_6H_4NO_2$-tpp) using $Zn(OAc)_2$.[3] Compound **4**

† Dedicated to Professor Rob Dunbar (Case Western Reserve University) on the occasion of his 60th birthday.

DOI: 10.1039/b202842p

Table 1 Crystal data for **4**(MeOH)·MeOH and **5**·$CHCl_3$

Empirical formula	$C_{53}H_{40}N_6O_5Zn$ [**4**(MeOH)·MeOH]	$C_{52}H_{33}Cl_4FeN_6O_3$ [**5**·$CHCl_3$]
Formula weight	906.28	987.49
Space group	*P*2(1)/*n*	*P*2(1)2(1)2(1)
Crystal system	Monoclinic	Orthorhombic
a/Å	14.865(3)	10.027(1)
b/Å	18.088(3)	17.277(2)
c/Å	16.773(3)	26.645(3)
β/°	97.200(4)	90
V/Å^3	4474(1)	4615.8(9)
Z	4	4
F(000)	1880	2020
μ(Mo Kα)/cm^{-1}	6.06	6.10
Crystal size/mm	0.63 × 0.50 × 0.25	0.32 × 0.25 × 0.25
T/K	295(2)	295(2)
No. of reflections measured	26251	29828
No. of reflections observed	9991 [$I > 2\sigma(I)$]	11062 [$I > 2\sigma(I)$]
R	0.0709	0.0501
R_w	0.2223	0.1115

was dissolved in $CHCl_3$ and layered with MeOH and dark blue crystals of **4**(MeOH)·MeOH were obtained for single crystal X-ray analysis. ^{1}H NMR (200.00 MHz, $CDCl_3$, 25 °C): δ 9.10 [d, H_β(5,14), ^3J(H–H) = 4.6 Hz], H_β(a,b) represents the two equivalent β-pyrrole protons attached to carbons a and b, respectively; 8.92 [d, H_β(4,15), ^3J(H–H) = 4.6 Hz]; 8.87 [s, H_β(9,10)]; 7.75–8.40 (m, phenyl protons); 7.79 [s, H_β(19,20)]; 6.63 [d, H_{NB}(48,50) or NB–$H_{3,5}$, ^3J(H–H) = 8.8 Hz], H_{NB}(c,d) represents the two equivalent protons attached to carbons c and d of *p*-nitrobenzoyl (NB) group respectively; 4.08 [d, H_{NB}(47,51) or NB–$H_{2,6}$, ^3J(H–H) = 8.8 Hz]. ^{13}C (150.92 MHz, $CDCl_3$, 25 °C): 162.3 [s, CO]; 151.4 (s) and 148.8 (s) for C_α(6,13) and C_α(3,16); 150.1 [s, C_α(8,11)]; 149.1 [s, C_α(1,18)]; 134.1 [s, C_β(5,14)]; 132.6 [s, C_β(9,10)]; 132.0 [s, C_β(4,15)]; 118.8 [s, C_β(19,20)]; 142.1 (s) and 141.9 (s) for phenyl-C_1[*i.e.*, C(21), C(27), C(33), and C(39)]; 135.5 (s), 135.1 (s), 134.4 (s), 128.5 (s), 128.0 (s), 127.5 (s), 126.9 (s) and 126.5 (s) for phenyl $C_{2,6}$, $C_{3,5}$, and C_4; 147.0 [s, C_{NB}(49) or NB–C_4]; 139.9 [s, C_{NB}(46) or NB–C_1]; 125.5 [s, C_{NB}(47,51) or NB–$C_{2,6}$]; 121.4 [s, C_{NB}(48,50) or NB–$C_{3,5}$]; 124.2 (s) and 122.9 (s) for C_m. MS, *m*/*z* (assignment, relative intensity): 842 ([Zn(N-*p*-$NCOC_6H_4NO_2$-tpp)]$^+$, 18.00), 840([Zn(N-*p*-$NCOC_6H_4NO_2$-tpp) − 2H]$^+$, 18.55), 692 ([Zn-(tpp) + N]$^+$, 15.57), 678 ([Zn(tpp)]$^+$, 75.96), 676 ([Zn(tpp)-2H]$^+$, 100.00). UV/visible spectrum, λ/nm ($\varepsilon \times 10^{-3}$/M^{-1} cm^{-1}) in MeOH: 435 (429.4), 566 (15.9), 606 (8.0).

Preparation of Fe(N-*p*-$NCOC_6H_4NO_2$-tpp)Cl (5)

A mixture of N-*p*-$HNCOC_6H_4NO_2$-Htpp (100 mg, 0.0136 mmol) in $CHCl_3$ (100 cm^3) and $FeCl_3$·$6H_2O$ (100 mg, 0.37 mmol) in MeOH (20 cm^3) was refluxed for 1 h. After concentrating, the residue was dissolved in $CHCl_3$ and filtered through a Celite pad. The filtrate was concentrated and the residue was recrystallized from $CHCl_3$–MeOH [1 : 1 (v/v)] yielding a dark blue solid of **5** (7.32 mg, 8.43 × 10^{-3} mmol, 62%). Compound **5** was dissolved in $CHCl_3$ and layered with MeOH to get the single-crystal for X-ray analysis. MS, *m*/*z* (assignment, relative intensity): 868 ([Fe(N-*p*-$NCOC_6H_4NO_2$-tpp)Cl]$^+$, 3.48), 704 ([Fe(tpp)Cl]$^+$, 8.18), 703 ([Fe(tpp)Cl − H]$^+$, 15.02), 669 ([Fe(tpp)]$^+$, 25.97), 668 ([Fe(tpp) − H]$^+$, 42.74). UV/visible spectrum, λ/nm ($\varepsilon \times 10^{-3}$/M^{-1} cm^{-1}) in $CHCl_3$: 358 (72), 422 (162), 521 (243), 696 (6.4).

NMR spectroscopy

^{1}H and ^{13}C NMR spectra were recorded at 599.95 and 150.87 MHz respectively on Varian Unity Inova-600 spectrometers locked on deuteriated solvent, and referenced to the solvent peak. ^{1}H NMR is relative to CD_2Cl_2 or $CDCl_3$ at δ = 5.30 or 7.24 and ^{13}C NMR to the center line of CD_2Cl_2 or $CDCl_3$ at δ = 53.6 or 77.0. HMQC (heteronuclear multiple quantum coherence) was used to correlate protons and carbon through one-bond coupling and HMBC (heteronuclear multiple bond coherence) for two- and three-bond proton–carbon coupling.

The positive-ion fast atom bombardment mass spectrum (FAB MS) was obtained in a nitrobenzyl alcohol (NBA) matrix using a JEOL JMS–SX/SX 102A mass spectrometer. UV/Visible spectra were recorded at 25 °C on a HITACHI U-3210 spectrophotometer.

Magnetic susceptibility measurements

The solid-state magnetic susceptibilities were measured under helium on a Quantum Design MPMS5 SQUID susceptometer from 5 to 300 K at a field of 1 T. The sample was held in a Kel-F bucket. The bucket had been calibrated independently at the same field and temperatures. The raw data for **5** were corrected for the molecular diamagnetism. The diamagnetic contribution of the sample was measured from an analogous diamagnetic metal complex, *i.e.* **4**(MeOH)·MeOH.

EPR spectroscopy

EPR spectra were measured on an X-band Bruker EMX-10 spectrometer equipped with an Oxford Instruments liquid helium cryostat. Magnetic field values were measured with an NMR gaussmeter and the frequency calibrated with a digital counter.

Crystallography

Table 1 presents the crystal data for **4**(MeOH)·MeOH and **5**·$CHCl_3$. Measurements were taken on a Siemens SMART CCD diffractometer using monochromated Mo-Kα radiation (λ = 0.71073 Å). The empirical absorption corrections were made for both complexes. The structures were solved by direct methods (SHELXTL PLUS)[32] and refined by the full-matrix least-squares method. All non-hydrogen atoms were refined with anisotropic thermal parameters, whereas all hydrogen atom positions were calculated using a riding model and were included in the structure factor calculation. Table 2 lists selected bond distances and angles for both **4**(MeOH)·MeOH and **5**.

CCDC reference numbers 182281 and 182282.

See http://www.rsc.org/suppdata/dt/b2/b202842p/ for crystallographic data in CIF or other electronic format.

Results and discussion

Molecular structures of 4(MeOH)·MeOH (*S* = 0) and 5 (*S* = 5/2)

The molecular framework is depicted in Fig. 1a for complex **4**(MeOH)·MeOH and in Fig. 1b for **5**·$CHCl_3$. Both the five-coordinate structures have metal atoms bonding with three

Table 2 Selected bond distances (Å) and angles (°) for compounds **4**(MeOH)·MeOH and **5**·$CHCl_3$

4(MeOH)·MeOH			
Zn(1)–N(1)	2.061(3)	Zn(1)–N(5)	2.035(3)
Zn(1)–N(2)	1.951(3)	Zn(1)–O(4)	2.106(3)
Zn(1)–N(3)	2.069(3)	Zn(1) ··· N(4)	2.564(3)
Zn(1)–O(4)–C(52)	131.9(4)	N(2)–Zn(1)–N(3)	94.3(1)
N(1)–Zn(1)–N(2)	94.6(1)	N(2)–Zn(1)–O(4)	111.4(2)
N(1)–Zn(1)–N(3)	169.7(1)	N(3)–Zn(1)–O(4)	87.4(1)
N(1)–Zn(1)–O(4)	94.2(1)		
5·$CHCl_3$			
Fe(1)–N(1)	2.086(3)	Fe(1)–N(5)	2.008(3)
Fe(1)–N(2)	1.979(3)	Fe(1)–Cl(1)	2.238(1)
Fe(1)–N(3)	2.078(3)	Fe(1) ··· N(4)	2.434(3)
Cl(1)–Fe(1)–N(1)	96.71(9)	N(1)–Fe(1)–N(3)	164.6(1)
Cl(1)–Fe(1)–N(2)	112.5(1)	N(1)–Fe(1)–N(5)	83.5(1)
Cl(1)–Fe(1)–N(3)	96.7(1)	N(2)–Fe(1)–N(3)	90.9(1)
Cl(1)–Fe(1)–N(5)	125.53(9)	N(2)–Fe(1)–N(5)	122.0(1)
N(1)–Fe(1)–N(2)	91.0(1)	N(3)–Fe(1)–N(5)	82.6(1)

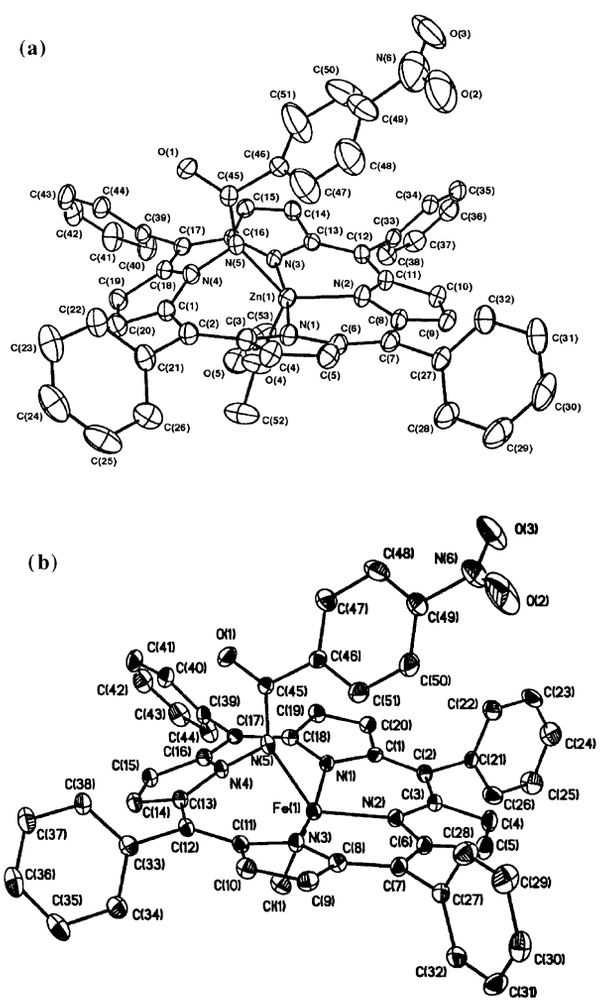

Fig. 1 Molecular configuration and atom-labeling scheme for (a) **4**(MeOH)·MeOH and (b) **5**·$CHCl_3$, with atomic displacement ellipsoids drawn at 30% probability. Hydrogen atoms for both compounds and the free solvent C(52)H(52A)Cl(2)Cl(3)Cl(4) for **5**·$CHCl_3$ are omitted for clarity. O(1) and O(1′) of **4**(MeOH)·MeOH are disordered with an occupancy factor of 0.7 for O(1) and 0.3 for O(1′).

nitrogen atoms of the porphyrins and one extra nitrogen atom of the nitrene fragment in common, but they are different with an axial MeOH ligand for **4**(MeOH)·MeOH and a Cl^- ligand in the axial site for **5**·$CHCl_3$. In both **4** and **5**, it appears that the *p*-nitrobenzoylimido (NNB) moiety is inserted into the Zn–N bond of (*meso*-tetraphenylporphyrinato)zinc(II), Zn(tpp),[9,10] and the Fe–N bond of chloro(*meso*-tetraphenylporphyrinato)iron(III), Fe(tpp)(Cl).[11] The unusual metal–ligand bond distances, *i.e.*, from the Zn(II) and Fe(III) atoms to the ligand and the angles are summarized in Table 2.

Bond distances (Å) are Zn(1)–O(4) = 2.106(3) and the mean Zn(1)–N(p) = 2.029(3) for **4**(MeOH)·MeOH; for **5** the values are Fe(1)–Cl(1) = 2.238(1) and the mean Fe(1)–N(p) = 2.048(3). The average Fe–N(p) distance of 2.048(3) Å in **5** is similar to that observed for the iron–pyrrole nitrogen bond of the high-spin (S = 5/2) iron(III) porphyrin complex Fe(N-NTs-tpp)Cl [Fe–N(p) = 2.036 Å], but it is substantially longer than the 1.990 Å value of intermediate-spin (S = 3/2) complexes.[4] The Zn(1)–O(4)(MeOH) distance of 2.106(3) Å is slightly longer than the sum of the covalent radii of Zn and O (1.93 Å) but is significantly shorter than the sum of the van der Waals radii of Zn and O (2.90 Å).[12] This Zn(1)–O(4) contact may be described as a weak covalent bond. The pyrrole nitrogen N(4) is no longer bonded to the zinc and iron as indicated by their longer internuclear distances, 2.564(3) Å for Zn(1) ··· N(4) and 2.434(3) Å for Fe(1) ··· N(4).

The distortion in these five-coordinate complexes can be quantified by the "degree of trigonality" which is defined as $\tau = (\beta - \alpha)/60$, where β is the largest and α the second largest of the L_{basal}–M–L_{basal} angles.[13,14] The limiting values are $\tau = 0$ for an ideal tetragonal geometry and $\tau = 1$ for an ideal trigonal-bipyramid. In the present case, we find β = 164.6(1)° [N(3)–Fe(1)–N(1)] and α = 125.33(9)° [N(5)–Fe(1)–Cl(1)] for **5**, and β = 169.7(1)° [N(3)–Zn–N(1)] and α = 130.5(1)° [N(2)–Zn–O(5)] for **4**(MeOH)·MeOH. Thus the value τ = 0.65 is obtained for both **4**(MeOH)·MeOH and **5**. Hence the geometries around Zn(II) in **4**(MeOH)·MeOH and Fe(III) in **5** are best described as a distorted trigonal bipyramid (or a square-based pyramidally distorted trigonal bipyramid, SBPDTBP)[15] with N(2), N(5), and O(4) [or N(2), N(5), and Cl(1)] lying in the equatorial plane for **4**(MeOH)·MeOH (or **5**). The τ values calculated for Fe(N-NTs-tpp)Cl[4] and Ga(N-NTs-tpp)(OAc)[6] by the same method are 0.72 and 0.68, respectively, and the coordination geometry for these two compounds is also distorted trigonal bipyramidal (or SBPDTBP). We adopt the plane of three strongly bound pyrrole nitrogen atoms [*i.e.*, N(1), N(2) and N(3)] as a reference plane, 3N.

Fig. 2 shows the actual porphyrin skeleton of **4**(MeOH)·MeOH and **5**. Because of the larger size of Fe^{3+}, Fe(1) lies 0.27 Å below the 3N plane toward the chlorine atom in **5**, compared to 0.09 Å for Zn(1) in **4**(MeOH)·MeOH [*cf.* 0.17 Å for Ni(II) in **1**, 1.15 Å for Tl(III) in **3**, and 0.21 Å for Fe(III) in Fe(N-NTs-tpp)Cl] (Fig. 2). The porphyrin macrocycle is indeed distorted because of the presence of the NB group (Fig. 2). Thus, the N(4) pyrrole rings bearing the NB group would mostly deviate from the 3N plane and orient separately in a dihedral angle of 30.0° for **4**(MeOH)·MeOH and 27.8° for **5**, whereas small angles of 17.7°, 9.3° and 13.0° occur with N(1), N(2), and N(3) pyrroles for **4**(MeOH)·MeOH and the corresponding angles are 6.3°, 2.1°, and 10.2° for **5**. In the diamagnetic compound **4**(MeOH)·MeOH, such a large deviation from planarity for the pyrrole N(4) is also reflected by observing a 13–15 ppm upfield shift in the ^{13}C NMR spectrum of the C_β (C19, C20) at 118.8 ppm compared to 134.1 ppm for C_β (C5, C14), 132.6 ppm for C_β (C9, C10), and 132.0 ppm for C_β (C4, C15). Similar upfield shifts were also observed for the diamagnetic complexes of C_β resonances due to the non-planarity of porphyrin with a magnitude of 12–19 ppm for Ni(N-*p*-$NCOC_6H_4NO_2$-tpp) and 17–21 ppm for Tl(N-*p*-$NCOC_6H_4NO_2$-tpp)(OAc).[7]

The pyrrole ring nitrogen N(4) is in fact inclined towards the Zn and Fe atoms in **4**(MeOH)·MeOH and **5**, respectively. These distortions make the distances between opposite pyrrole nitrogen atoms unusual. The normal diameter of the "hole" in an

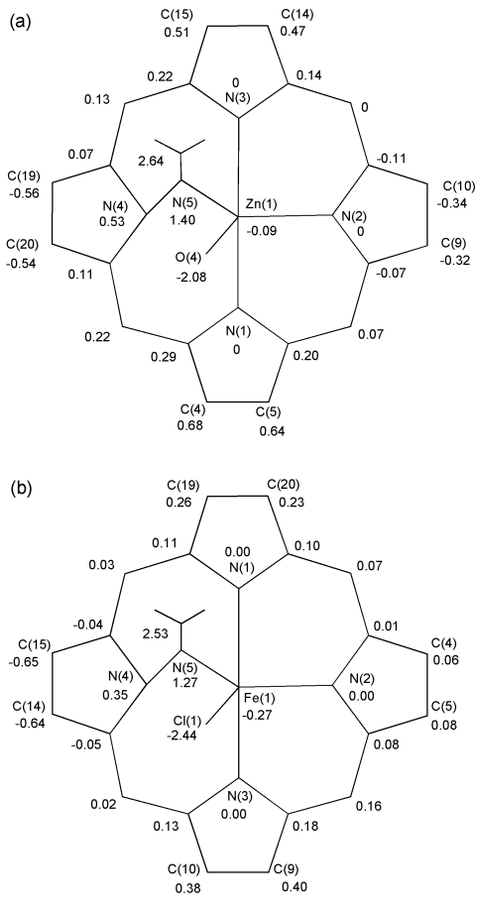

Fig. 2 Diagram of the porphyrinato core ($C_{20}N_4$, M, NB, Cl^-, and OMe) of (a) compound **4**(MeOH)·MeOH and (b) compound **5**. The values represent the displacements (in Å) of the atoms from the mean 3N plane [*i.e.*, N(1), N(2) and N(3) for **4**(MeOH)·MeOH and **5**].

undistorted metalloporphyrin complex has been estimated to be 4.02 Å.[16] The N(2) ··· N(4) distances of 4.468 Å in **4**(MeOH)·MeOH and of 4.328 Å in **5** are unusually long, which is caused by the large deviation of the N(4) pyrrole in **4**(MeOH)·MeOH and **5** from the 3N plane. Because of this distortion, the N(1) ··· N(3) distance is 4.113 Å in **4**(MeOH)·MeOH and 4.126 Å in **5**. Hence, in **4**(MeOH)·MeOH(or **5**), the zinc(II) [or iron(III)] atom is bound in an expanded porphyrinato (4N) core. The plane (P) defined by Zn(1), N(5), N(4), and C(45) in **4**(MeOH)·MeOH, or by Fe(1), N(5), N(4), and C(45) in **5** is almost perpendicular to the 3N plane with an angle of 94.1° in **4**(MeOH)·MeOH and 79.9° in **5**. The *p*-nitrobenzoyl group (NB) [*i.e.*, the plane for NB is C(46)–C(51)] is bonded to N(5) in **4**(MeOH)·MeOH and **5** so that it lies above the macrocycle, orienting in a dihedral angle of 47.9° and 61.3° with the 3N plane in **4**(MeOH)·MeOH and **5**, respectively. The dihedral angles between the mean plane of the skeleton (3N) and the planes of the phenyl groups are 46.1° [C(24)], 49.3° [C(30)], 58.0° [C(36)], and 46.5° [C(42)] for **4**(MeOH)·MeOH and the corresponding angles are 44.0°, 78.7°, 87.4°, and 42.2° for **5**.

Magnetic properties of complex 5

The temperature dependence of the molar magnetic susceptibility, χ_M, and magnetic moment, μ_{eff}, of the crystalline complex **5** is shown in Fig. 3. As can be seen in Fig. 3, the value of μ_{eff} varies from 5.87 μ_B at 300 K to 4.28 μ_B at 5 K. The magnetic moment clearly shows a plateau equal to 5.87 μ_B at high temperatures (300–50 K), which is close to the expected value of 5.92 μ_B for a sextuplet high-spin state ($S = 5/2$). Below 20 K, the magnetic moment drops rapidly, reflecting the large zero-field splitting of the ground state which is usual in high-spin iron(III) porphyrins.[17,18]

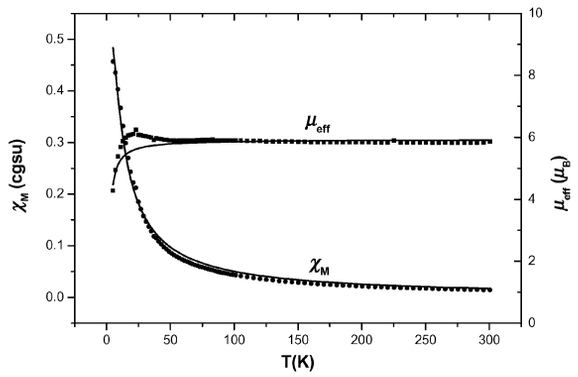

Fig. 3 Temperature dependence of the molar paramagnetic susceptibility, χ_M, and the magnetic moment, μ_{eff}, for a microcrystalline sample of **5** in the range 5–300 K. Points are the experimental data; solid lines represent the least-squares fit of the data to eqn. (3).

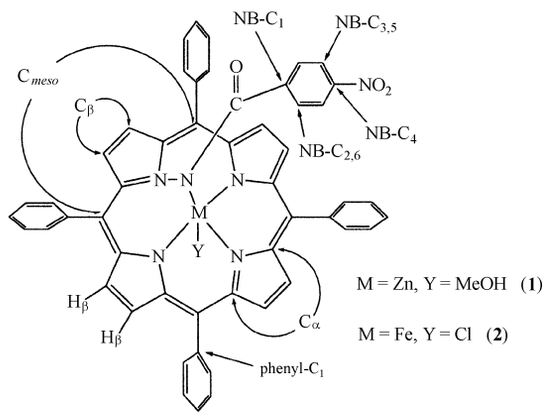

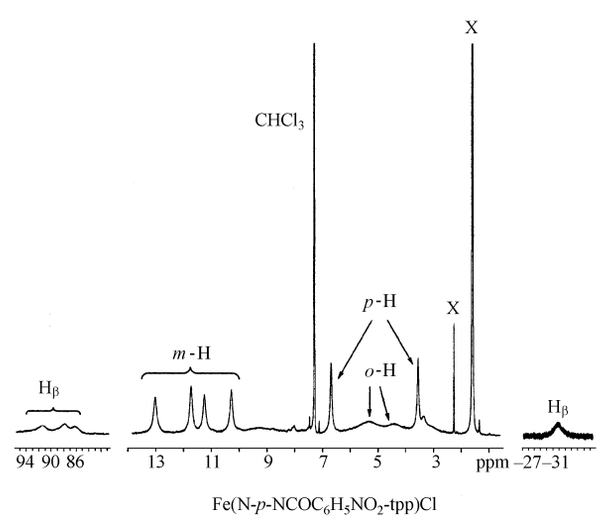

Fig. 4 ^{1}H NMR spectrum of **5** at 599.95 MHz in $CDCl_3$ at 20 °C.

^{1}H NMR spectroscopy of 5 in solution

The ^{1}H NMR spetrum of **5** in $CDCl_3$ at 20 °C is shown in Fig. 4. The signals at 92.22, 88.11, 86.22, and −31.34 ppm have been assigned to the pyrrole protons (H_β). These four signals for H_β indicate that complex **5** has effective C_s symmetry in solution with a mirror plane running through the Cl(1)–Fe(1)–N(2)–N(5)–N(4) unit. The signals at 13.21, 11.89, 11.39, and 10.40 ppm are due to the *meta* protons of the phenyl group (*m*-H). The signals at 6.69, and 3.45 ppm are assigned to the *para* protons of the phenyl rings (*p*-H). The two broad signals at 5.35 and 4.35 ppm have been assigned to the *ortho* protons of the phenyl group (*o*-H), which are closer to the paramagnetic center compared to the *meta* protons. Thus, the NMR spectra show clear evidence of spin density delocalization onto the

ligand for the Fe(III) complex, giving the so-called contact shifts for the ^{1}H spectra.[19,20] Since signal assignment of the ^{13}C NMR data is not simple for compound **5**, it is difficult to see whether this spin delocalization effect is present in the ^{13}C spectra or not.

EPR spectra of 5

The spin Hamiltonian (H_s, $S = 5/2$) used to interpret the EPR data is[21–23]

$$H_s = H_z + H_{CF} \quad (1)$$

where

$$H_z = g\mu_B HS$$
$$H_{CF} = D\,[S_z^2 - S(S+1)/3] + E(S_x^2 - S_y^2)$$

The first term H_z in the spin Hamiltonian (H_s) is the electronic Zeeman term, which describes the interaction of the electronic spin S, with the external magnetic field H. H_{CF} is the crystalline electric field, μ_B is the Bohr magneton, g is the electronic g-tensor, and D and E are the axial and rhombic zero-field splitting (ZFS) parameters.

The rhombicity parameter, λ (= E/D), is a measure of the departure of the electronic environment of the iron center from axial symmetry. In an appropriate axis system, axial symmetry correponds to $\lambda = 0$ while a maximally rhombic symmetry corresponds to $\lambda = 1/3$.[24,25] For $D \gg h\nu$ (the energy of the microwave, ~0.32 cm^{-1} at X-band), the three Kramers doublets of a $S = 5/2$ system act approximately like independent "$S = 1/2$" systems with effective g-values that are dependent only on λ.

The high degree of rhombicity of the iron center in **5** is demonstrated by the presence of the intense signal at $g = 4.2$ in a powdered solid, as shown in Fig. 5. In the solid-state spectra,

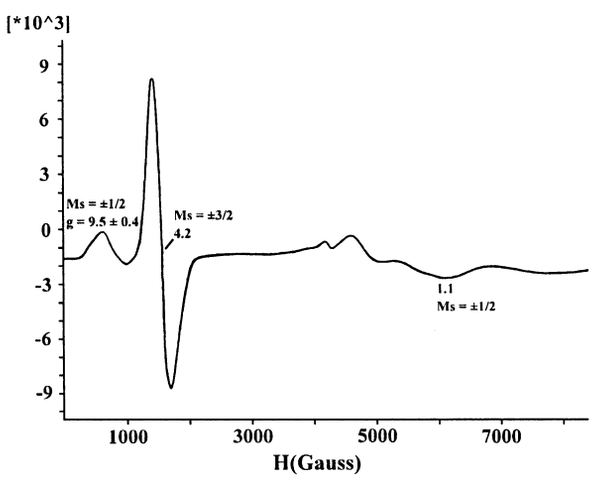

Fig. 5 Solid-state X-band EPR spectrum of a finely powdered sample of **5** at 4 K. EPR conditions: microwave frequency 9.466 GHz; modulation amplitude 1.60 G; modulation frequency 100.00 kHz; microwave power 1.997 mW.

a shoulder was observed on the large ($g = 4.2$) signal at approximately $g = 9.5 \pm 0.4$. A weak transition was also observed in the region near $g = 1.1$. From plots of the effective g values *versus* λ, we conclude that $\lambda = E/D = 0.29$ for complex **5** which is 87% towards complete rhombicity.[21,26–29] According to this analysis, the prominent signal at $g = 4.2$ arises from the middle Kramers doublet with "$M_s = \pm 3/2$", while the weaker signal at $g = 9.5 \pm 0.4$ results from the lowest Kramers doublet with "$M_s = \pm 1/2$". The resonance at $g = 1.1$ corresponds to transitions in the lowest (or ground) Kramers doublet with "$M_s = \pm 1/2$". Moreover the "rhombicity" of the iron d orbitals had not been reported for complex Fe(N-NTs-tpp)Cl.[4,30]

A reasonable estimate of the principal g values associated with the middle doublet may be obtained by using the minimum, maximum, and inflection points of the $g = 4.2$ EPR absorption derivative as limits for the g values.[27] The g value for the maximum ($g = 4.6$), minimum ($g = 3.9$), and inflection point ($g = 4.2$) of the main signal at $g = 4.2$ were close to the calculated values of $g_{2z} = 4.53$, $g_{2y} = 4.03$, and $g_{2x} = 4.24$ derived from the transitions in the middle Kramers doublet (Fig. 6). As

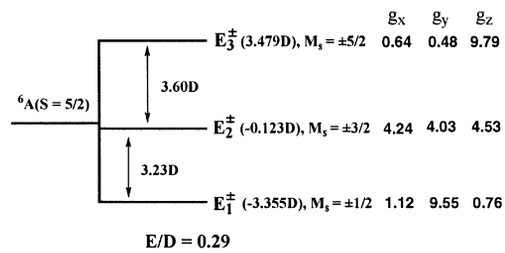

Fig. 6 Schematic representation of the energy levels for **5** with an $S = 5/2$ system for $E/D = 0.29$ and the spin Hamiltonian (1), where $E_i^{\pm}$ represents the energy of the three Kramers doublets with $i = 1, 2, 3$ for the ground (the lowest), middle, and uppermost doublets, respectively.

shown in Figs. 5 and 6, the g values with $g_{1x} = 1.12$ and $g_{1y} = 9.55$ calculated for the lowest Kramers doublet indeed agree semi-quantitatively with observed $g_{1x} = 1.1$ and $g_{1y} = 9.5 \pm 0.4$. The eigenfunctions and energies of eqn. (1) with $\lambda = 0.29$ in zero field (for $D > 0$) are

$$\begin{aligned}
|\phi_1^{\pm}> &= -0.1237\,|\pm 5/2> + 0.902\,|\pm 1/2> -0.4129\,|\mp 3/2> \\
|\phi_2^{\pm}> &= -0.1065\,|\pm 5/2> + 0.4017\,|\pm 1/2> +0.9096\,|\mp 3/2> \\
|\phi_3^{\pm}> &= 0.9865\,|\pm 5/2> + 0.1568\,|\pm 1/2> +0.0465\,|\mp 3/2> \\
E_1^{\pm} &= -3.355D \\
E_2^{\pm} &= -0.123D \\
E_3^{\pm} &= 3.479D
\end{aligned} \quad (2)$$

and they are shown schematically in Fig. 6.[31]

The paramagnetic susceptibility, χ_M, and effective magnetic moment, μ_{eff}, data shown in Fig. 3 for **5** were least-squares which fit to eqn. (3) to give the fitting parameters $D = 0.79$ cm^{-1} and $g = 2.39$.

$$\chi_M = \frac{Ng^2\beta^2}{4kT}\left[\frac{0.14 + 5.12e^{-3.23X} + 23.85e^{-6.83X}}{1 + e^{-3.23X} + e^{-6.83X}}\right] \quad (3)$$

In eqn. (3), $X = D/kT$, g is the average g value, and the other symbols have their usual meanings. Eqn. (3) is the simple theoretical susceptibility equation resulting from the axial and rhombic zero-field splitting (ZFS) for $S = 5/2$ as governed by the spin Hamiltonian H_s in eqn. (1). Importantly, the energy splitting diagram for **5** with $\lambda = 0.29$ shown in Fig. 6 and the eigenfunctions shown in eqn. (2) are used in the derivation of eqn. (3). The solid lines in Fig. 3 represent this fit. This value of D means that the relative energies of the three Kramer doublets at zero magnetic field are 0, 2.55, and 5.40 cm^{-1}.

On consideration of all the experimental data combined, *i.e.*, the magnetic moment $\mu = 5.92\ \mu_B$ at 300–50 K, the EPR signals at $g = 9.5 \pm 0.4$, 4.2, and 1.1 at 4 K, the Fe–N(p) distance 2.048(1) Å at 22 °C, and NMR shifts of the pyrrole protons (H_β) ($\delta = 92.22$, 88.11, 86.22, −31.34) at 20 °C firmly establish a high-spin ($S = 5/2$) state for complex **5**. Although the characteristics of complex **5** are similar to those previously reported for the high-spin pentacoordinate iron(III) porphyrin complex Fe(N-NTs-tpp)Cl,[4] the fine structure of the EPR signals and paramagnetic susceptibility data allow us unambiguously to evaluate the parameters $\lambda = 0.29$ and $D = 0.79$ cm^{-1} for **5**. This is

the first report applying the rhombicity evaluation by EPR methods to bridged metalloporphyrins with a Fe–NNB–N likage.

In conclusion, we have investigated two pentacoordinate [one diamagnetic, **4**(MeOH)·MeOH, and one paramagnetic, **5**], mononuclear, and bridged metal complexes of *N*-*p*-nitrobenzoylamido-*meso*-tetraphenylporphyrin having a M–NNB–N [M = Zn(II), Fe(III)] linkage, and established their X-ray structures. X-Band EPR spectroscopy and solid-state magnetic susceptibility data can be used to assess the zero-field splitting, D, and the rhombicity parameter, λ (= E/D), for **5**.

Acknowledgements

Financial support from the National Science Council of the R.O.C. under Grant NSC 90-2113-M-005-014 is gratefully acknowledged. The NMR instrument (Varian Unity Inova-600) was funded in part by the National Science Council and by the Chung-Cheng Agriculture Science & Social Welfare Foundation.

References

1 J. C. Setsune, Y. Kishimoto, Y. Ishimaru, K. Fukuhara and T. Kiato, *Organometallics*, 1991, **10**, 1099.
2 Y. I. Li, C. S. Chang, J. Y. Tung, C. H. Tsai, J. H. Chen, F. L. Liao and S. L. Wang, *Polyhedron*, 2000, **19**, 413.
3 H. J. Callot, B. Chevrier and R. Weiss, *J. Am. Chem. Soc.*, 1978, **100**, 4733.
4 J. P. Mahy, P. Battioni, G. Bedi, D. Mansuy, J. Fishcher, R. Weiss and I. Morgenstern-Badarau, *Inorg. Chem.*, 1988, **27**, 353.
5 H. J. Callot, B. Chevrier and R. Weiss, *J. Am. Chem. Soc.*, 1979, **101**, 7729.
6 J. Y. Tung, J. I. Jang, C. C. Lin, J. H. Chen and L. P. Hwang, *Inorg. Chem.*, 2000, **39**, 1106.
7 C. S. Chang, C. H. Chen, Y. I. Li, B. C. Liau, B. T. Ko, S. Elango, J. H. Chen and L. P. Hwang, *Inorg. Chem.*, 2001, **40**, 2905.
8 P. J. Kellett, M. J. Powlik, L. F. Taylor, R. G. Thompson, M. A. Lerstik, O. P. Anderson and S. H. Strauss, *Inorg. Chem.*, 1989, **28**, 440.
9 R. J. Abraham, G. R. Bedford, G. R. McNeillie and B. Wright, *Org. Magn. Reson.*, 1980, **14**, 418.
10 D. F. Marsh and L. M. Mink, *J. Chem. Educ.*, 1996, **73**, 1188.
11 H. J. Callot, B. Chevrier and R. Weiss, *J. Am. Chem. Soc.*, 1978, **100**, 4733.
12 J. E. Huheey, E. A. Keiter and R. L. Keiter, *Inorganic Chemistry*, Harper Collins College Publishers, New York, 4th edn., 1993, p. 114.
13 A. W. Addison, T. N. Rao, J. Reedijk, J. V. Rijn and G. C. Verschoor, *J. Chem. Soc., Dalton Trans.*, 1984, 1349.
14 R. G. Garvey, R. O. Koob and M. L. Morris, *Acta Crystallogr., Sect. C*, 1987, **43**, 2056.
15 G. Murphy, P. Nogle, B. Murphy and B. Hathaway, *J. Chem. Soc., Dalton Trans.*, 1997, 2645.
16 D. M. Collins and J. L. Hoard, *J. Am. Chem. Soc.*, 1970, **92**, 3761.
17 S. Mitra, in *Iron Porphyrins part II*, eds. A. B. P. Lever and H. Gray, Addison-Wesley, Reading, MA, 1983, p. 1.
18 M. Mazzanti, J. C. Marchon, J. Wojaczyski, S. Wolowiec, L. Lotos-Grazynski, M. Shang and W. R. Scheidt, *Inorg. Chem.*, 1998, **37**, 2476.
19 F. H. Kohler, in *Magnetism: Molecules to Materials, Models and Experiments*, eds. J. S. Miller and M. Drillon, Wiley–VCH, Weinheim, 2001, p. 379.
20 R. S. Drago, *Physical Methods for Chemists*, Saunders College Publishing, New York, 2nd edn., 1992, pp. 507–542.
21 (*a*) H. H. Eickman, M. P. Klein and D. A. Shirley, *J. Chem. Phys.*, 1965, **42**, 2113; (*b*) W. R. Hagen, *Adv. Inorg. Chem.*, 1992, **38**, 165.
22 B. J. Graffney and H. J. Silverstone, in *Biological Magnetic Resonance in EMR of Paramagnetic Molecules*, eds. J. Berliner and J. Reuben, Plenum Press, New York, 1993, vol. 13, pp. 1–57.
23 K. Spartalian, W. T. Oosterhuis and J. B. Neilands, *J. Chem. Phys.*, 1975, **62**, 3538.
24 W. E. Blumberg, in *Magnetic Resonance in Biological Systems*, eds. A. Ehrenberg, B. G. Malmstrom and T. Vanngard, Pergamon Press, Oxford, 1967, pp. 119–133.
25 P. L. Hall, B. R. Angle and J. P. E. Jones, *J. Magn. Reson.*, 1974, **15**, 64.
26 A. J. Simaan, F. Banse, P. Mialane, A. Boussac, S. Un, T. Kargar-Grisel, G. Bouchoux and J. J. Girerd, *Eur. J. Inorg. Chem.*, 1999, 993.
27 J. N. Burstyn, J. A. Roe, A. R. Miksztal, B. A. Shuevitz, G. Lang and J. S. Valentine, *J. Am. Chem. Soc.*, 1988, **110**, 1382.
28 Y. Deligiannakis, A. Boussac, H. Bottin, V. Perrier, O. Barzu and A. M. Gilles, *Biochemistry*, 1997, **36**, 9446.
29 J. Peisach, W. E. Blumberg, E. T. Lode and M. J. Coon, *J. Biol. Chem.*, 1971, **246**, 5877.
30 E. I. Solomon, J. Zhou, F. Neese and E. G. Pavel, *Chem. Biol.*, 1997, **4**, 495.
31 A. X. Trautwein, E. Bill, E. L. Bominaar and H. Winkler, *Struct. Bonding (Berlin)*, 1991, **78**, 1.
32 G. M. Sheldrick, SHELXTL PLUS, Bruker Analytical X-Ray Instruments, Madison, WI, 1990.